HHS Public Access

Author manuscript

Dev Dyn. Author manuscript; available in PMC 2016 April 01.

Published in final edited form as:

Dev Dyn. 2015 April ; 244(4): 607–618. doi:10.1002/dvdy.24246.

Using optical coherence tomography to rapidly phenotype and quantify congenital heart defects associated with prenatal alcohol exposure

Ganga Karunamuni[1], **Shi Gu**[2], **Yong Qiu Doughman**[1], **Amanda I. Noonan**[2], **Andrew M. Rollins**[2], **Michael W. Jenkins**[1], and **Michiko Watanabe**[1]

[1]Department of Pediatrics, Case Western Reserve University, 11100 Euclid Avenue, Cleveland, OH 44106, USA

[2]Department of Biomedical Engineering, Case Western Reserve University, 11100 Euclid Avenue, Cleveland, OH 44106, USA

Abstract

Background—The most commonly used method to analyze congenital heart defects involves serial sectioning and histology. However, this is often a time-consuming process where the quantification of cardiac defects can be difficult due to problems with accurate section registration. Here we demonstrate the advantages of using optical coherence tomography, a comparatively new and rising technology, to phenotype avian embryo hearts in a model of Fetal Alcohol Syndrome where a binge-like quantity of alcohol/ethanol was introduced at gastrulation.

Results—The rapid, consistent imaging protocols allowed for the immediate identification of cardiac anomalies, including ventricular septal defects and misaligned/missing vessels. Interventricular septum thicknesses and vessel diameters for three of the five outflow arteries were also significantly reduced. Outflow and atrio-ventricular valves were segmented using image processing software and had significantly reduced volumes compared to controls. This is the first study to our knowledge that has 3-D reconstructed the late-stage cardiac valves in precise detail in order to examine their morphology and dimensions.

Conclusion—We believe therefore that OCT, with its ability to rapidly image and quantify tiny embryonic structures in high resolution, will serve as an excellent and cost-effective preliminary screening tool for developmental biologists working with a variety of experimental/disease models.

Keywords

biophotonic; heart; defects; alcohol; ethanol; embryo

Corresponding author: Ganga Karunamuni, 11100 Euclid Avenue, Wearn 448, Cleveland, Ohio 44106. ghk6@case.edu, phone: 216-844-7229..

Introduction

For many developmental biology researchers, the gold standard method for phenotyping embryos in order to investigate anomalies such as congenital heart defects involves serial sectioning and histology. However, this process has several drawbacks. First, it consumes time and effort especially if there are large cohorts of embryos to be analyzed. Serial sectioning is compromised if sections are lost, thus requiring a high level of skill to capture the sections. In addition, analysis of cardiac structures and any related defects depends a great deal on the orientation of the sample and the plane of the section, thereby complicating the comparison of embryos. Finally, analysis through histopathology does not usually involve the quantification of observed defects since 3-D reconstruction of embryonic tissues can be difficult due to problems with section registration. Even episcopic fluorescent imaging capture (EFIC), which involves the embedding of samples in paraffin and automated image collection (Weninger and Mohun, 2002; Rosenthal et al., 2004; Weninger and Mohun, 2007; Geyer et al., 2009; Mohun and Weninger, 2012), can take up substantial time especially when dealing with large sample sizes. It may therefore be beneficial to consider other technologies in order to streamline the investigation of high throughput animal models with complex and possibly subtle defects during development. Non-destructive 3-D imaging tools can be extremely valuable in providing a more comprehensive, objective analysis of potential congenital defects while allowing the use of further assays.

Currently there are multiple imaging modalities that could complement the histological examination of embryonic models. Ultrasound is commonly used in the research community, due to its relatively large imaging depth, its non-invasive high throughput nature, and its ability to reliably interrogate cardiovascular function (Yu et al., 2004; Shen et al., 2005; Spurney et al., 2006; deAlmeida et al., 2007; McQuinn et al., 2007; Tobita et al., 2010; Simpson and Miller, 2011). However, the analysis of cardiac structures is complicated by its limited 2-D imaging resolution (440 μm axial resolution). Ultrasound biomicroscopy, a new development in the field, has improved axial resolution (30 μm) compared to clinical ultrasound systems but is not quite ready for high throughput applications because of the longer scanning protocol (Tobita et al., 2010; Moran et al., 2013). Micro-computed tomography (micro-CT) is also non-destructive but has better imaging resolutions (10-15 μm) than ultrasound (Degenhardt et al., 2010; Schambach et al., 2010; Tobita et al., 2010; Cheng et al., 2011; Ritman, 2011), thus improving on the visualization of cardiac anatomy. The technology is limited though by inconsistencies in sample staining with contrast agents which can compromise the quality and resolution of the imaging (Cheng et al., 2011; Hiraiwa et al., 2013). Furthermore, tiny structures like the cardiac valves cannot be visualized in detail using micro-CT without the use of high-resolution systems that can add substantially to image acquisition and image processing times. Another non-invasive technology that has been used frequently for imaging animal models is micro-MRI (Yelbuz et al., 2004; Petiet et al., 2008; Berrios-Otero et al., 2009; Cleary et al., 2009; Hogers et al., 2009; French et al., 2010; Nieman and Turnbull, 2010; Tobita et al., 2010; Zouagui et al., 2010). This method can provide relatively high resolution images (20-25 μm) without using contrast agents or harmful radiation like micro-CT. The investigation of multiple samples

however would potentially be limited by the scanning time of micro-MRI, which often involves several hours on average (Liu et al., 2013). Other cutting-edge technologies such as optical projection tomography and lightsheet fluorescence microscopy are advancing the field of fluorescence visualization while eliminating the problems of photo-toxicity or bleaching that can often occur during confocal or multi-photon microscopy (Konig, 2000; Sharpe et al., 2002; Pawley, 2006; Santi, 2011; Swoger et al., 2014). To summarize, there are many modalities with their own benefits and limitations that have been adapted for the initial analysis of cardiac defects in small animal models. In this study, we will illustrate the promising potential of optical coherence tomography (OCT) as a rapid, accessible, non-expensive tool for such preliminary screening applications.

OCT imaging is based upon low-coherence interferometry with high spatial resolution (2-20 μm) and penetration depths (1-3 mm), lying between ultrasound and confocal microscopy with regards to these parameters (Drexler and Fujimoto, 2008a). In clinical applications, OCT has been frequently used in ophthalmology to quickly assess the retina in a non-invasive setting and may have potential as a guidance tool during eye surgery (Drexler and Fujimoto, 2008b; Fernandez et al., 2008; Ide et al., 2010; Tao et al., 2010; Sohrab and Fawzi, 2013). In addition, intravascular OCT (IVOCT) is used by interventional cardiologists to analyze the coronaries for inflammation and atherosclerosis, as well as guide and verify stent placement (Prati et al., 2011; Tearney et al., 2012; Asrar Ul Haq et al., 2013; Ferrante et al., 2013; Vignali et al., 2014). We, as well as others, have customized OCT technology in order to investigate the structure and function of the embryonic heart (Gu et al., 2011; Jenkins et al., 2012). Since OCT is non-invasive, this allows for longitudinal observations of hearts belonging to avian embryos that have been cultured in plastic culture dishes under physiological conditions (humidified, temperature-controlled chamber) (Happel et al., 2011; Jenkins et al., 2012). To date, OCT studies of cardiac development have focused mostly on the early-stage looping heart at a time when the cardiac cushions are still developing and when the outflow tract has not yet septated into its major branching arteries (Yelbuz et al., 2002a; Yelbuz et al., 2002b; Jenkins et al., 2007a; Jenkins et al., 2007b; Davis et al., 2008; Larina et al., 2008; Rugonyi et al., 2008; Garita et al., 2011; Liu et al., 2012; Karunamuni et al., 2014). In earlier studies from our group, embryos that had been exposed to binge volumes of ethanol at gastrulation were found to exhibit altered cardiac function and structure at early developmental stages as detected by OCT imaging (Karunamuni et al., 2014). Histopathology also revealed that ethanol-exposed embryos developed congenital heart defects (CHDs) associated with Fetal Alcohol Syndrome (FAS), including valvular and septal defects (Karunamuni et al., 2014) which have been observed in different ethanol exposure models (Daft et al., 1986; Sulik et al., 1986; Fang et al., 1987; Bruyere and Stith, 1993; Serrano et al., 2010). Almost all these previous findings have been qualitative rather than quantitative, relying on microscopy or histological analysis for the identification of defects. This manuscript focuses on the late-stage embryonic heart where the normal heart has fully septated into four distinct chambers with cardiac valves, and the outflow tract has branched into its major vessels, thereby reflecting the mature cardiac phenotype. We used OCT for the first time to define and measure late-stage cardiac parameters that can be clinically significant as diagnostic markers and predictors of future outcomes. Our findings not only add to the body of work supporting the prevalence of

alcohol-induced CHDs, but also provide more detailed information about the scope and variability of these defects. Our methods could be instrumental as well in sensitively probing for mechanisms of teratogenicity and assessing the efficacy and safety of protocols for CHD prevention.

Results

In brief, the ethanol exposure experiments were performed using an avian model where quail eggs were incubated until HH Stage 4-5 (gastrulation), when the embryo is vulnerable to the induction of CHDs (Serrano et al., 2010; Karunamuni et al., 2014). At this stage, experimental eggs were injected with 40 μl of 50% ethanol (in saline) and control eggs were either injected with 40 μl of saline or left intact. Ethanol dosage was based on previous studies (Fang et al., 1987; Bruyere and Kapil, 1990; Bruyere et al., 1994; Serrano et al., 2010) as being equivalent to one binge drinking episode (4-5 drinks at one time) in humans. The cohort described in this study included 17 total controls and 23 total ethanol-exposed embryos (Table 1) and were collected at Embryonic Day 8 (HH Stage 34) (Hamburger and Hamilton, 1951). All embryos were similar in size and were staged. Most controls survived to this developmental time-point, with a survival rate of 82% (14/17). All of the surviving control embryos had no observed defects of the head or body and had fully septated hearts with the aortic trunk branching into the right brachiocephalic artery (RBA), left brachiocephalic artery (LBA), and aortic arch (AA), and the pulmonary trunk branching into the right pulmonary artery (RPA) and left pulmonary artery (LPA). In comparison, ethanol exposure resulted in lower survival rates (52%; 12/23) and 42% (5/12) of the survivors developed gross morphological defects, where the cranial folds failed to fuse and/or the chest wall failed to fuse (Figure 1, Tables 1 and 2). Such gross malformations and decreases in embryo viability are characteristic defects of the embryonic ethanol exposure model (Memon and Pratten, 2009). Further analysis of the OCT images of the embryo hearts revealed that 58% (7/12) of the ethanol-exposed embryos exhibited a spectrum of obvious cardiac defects, ranging from perimembranous and muscular ventricular septal defects (VSDs), missing or misaligned great vessels, double outlet right ventricle (DORV), and hypoplastic or abnormally rotated ventricles (Tables 1 and 2). These defects were noted during the first fly-through of the OCT images using image processing software (AMIRA). Interestingly, all five experimental embryos that developed gross malformations also exhibited cardiac defects but there were also two apparently normal looking embryos that presented with CHDs. In fact, Ethanol Embryo #2 that had defects in both the head and body (Table 2) developed only a VSD whereas Ethanol Embryo #9, while appearing to have a normal head and body, had multiple cardiac anomalies. Thus the lack of body defects may not necessarily indicate an absence of CHDs in the FAS model.

Overall the most commonly occurring cardiac defect after ethanol exposure was the presence of a VSD, which was exhibited by 5/12 embryos (42%) (Table 2). Analysis of OCT images allowed for rapid identification of these malformations (Figure 2 A-B), and subsequent measurements were also taken of the interventricular septum (IVS) thickness using AMIRA tools. The IVS thickness was consistently measured at a similar level in the heart across multiple embryos using ubiquitous landmarks (Figure 2 C, inset in panel D), and was found to be significantly reduced (32% decrease in thickness, $p < 0.05$) in ethanol-

exposed embryos (Figure 2 D). Another frequently seen CHD (3/12 embryos, 25%) was the absence of one of the five major branches of the outflow vessels at this level (Tables 1 and 2): either the RPA or the RBA (Table 2, Figure 3 A-C). When the ventral-dorsal lumen diameter was measured for each for the five branching arteries, dimensions for the LBA, the RBA and the AA, that is the aortic branches, were found to be significantly reduced after ethanol exposure (14% decrease, 16% decrease and 18% decrease in diameter respectively, $p < 0.05$) (Figure 3 D). Outer diameters for the LBA, RBA and AA were also significantly reduced (6% decrease, 12% decrease and 10% decrease in diameter respectively, $p < 0.05$), indicating that the entire vessel was smaller, perhaps a consequence of altered flow in those arteries. There was a similar trend of reduction for the pulmonary artery diameters but the difference was not statistically significant (Figure 3 D). There were no significant changes in vessel wall thickness for any of the five major branching arteries when they were present.

Valvular phenotypes can often be overlooked in disease models especially using other imaging modalities which may not have the resolution to image these small yet complex and critical structures. This is unfortunate since abnormal valve morphology and orientation can yield pertinent information about cardiac function at a particular developmental time-point (Serrano et al., 2010). In our studies, the pulmonary valve was easily identified in OCT cross-sections of the heart (Figure 4 A-C) and segmented in AMIRA, although the individual leaflets could not be delineated since they were too tightly apposed. Total valvular volume was reduced by 24% ($p < 0.05$) in ethanol-exposed embryos (Figure 4 D), suggesting that outflow function may be impaired at this stage. Unfortunately, the aortic valve leaflets are not completely visible due to the deep location of the aorta behind multiple tissue structures. The left atrio-ventricular (AV) valve leaflets, also termed the mitral valve, were easily distinguished as well using OCT and were segmented (Figure 5 A). Typically in control hearts, after dissection and treatment with potassium chloride which relaxes the heart tissue, the longer septal leaflet and the stubby mural leaflet for the left AV valve are in contact with each other in a V-shaped orientation (Figure 5 B). Two embryos in the ethanol cohort exhibited abnormal valve morphology, an example of which is presented in Figure 5 C, where the leaflets do not touch at all. This particular heart belonged to Ethanol Embryo # 2 which developed both cranial and chest wall defects (Table 2). In addition, volumes for the septal AV leaflet and mural AV leaflet in the ethanol-exposed group were reduced by 46% and 42% respectively ($p < 0.05$), while total leaflet volume was reduced by 45% (Figure 5 D). It is expected that such drastic changes in valve volume or morphology could compromise left AV function, perhaps leading to increased regurgitation and thus impairing blood flow to the rest of the body. The right AV valve was not analyzed in these embryos because in the avian it is composed of muscular tissue instead of the normal valvular cell types (Lu et al., 1993), and thus the valvular borders could not be clearly distinguished from the myocardial wall for segmentation in OCT images with the current technology. This may be feasible in the future with continual improvements to the instrumentation and post-processing protocol.

Discussion

With the use of high-resolution OCT technology, the analysis for FAS-associated CHDs in the avian model proved to be quite illuminating. Not only did we observe the increased

frequency of VSDs and great vessel defects as seen in other FAS models (Daft et al., 1986; Sulik et al., 1986; Fang et al., 1987; Bruyere and Stith, 1993; Serrano et al., 2010), but for the first time we were also able to rapidly and precisely identify and quantify changes in structure (vessel diameter, IVS thickness and valve volume) that could have been difficult to detect and quantify using other methodologies. The entire analysis process was streamlined dramatically, especially for a cohort of this size (26 embryos in total). Typically with histopathological phenotyping, embryo hearts would be collected on the day of interest, fixed for 2-3 hours in paraformaldehyde, incubated in sucrose (a cryo-protectant) overnight, and then sectioned on the following day with microscopy analysis afterwards in order to identify potential defects. This procedure can be quite time-consuming when dealing with a large batch of samples, often ranging from a few days to a few weeks. Quantification of tissue structures would be difficult, and there may also be inconsistencies in the comparison of different embryos, due to differences in sectioning orientation. For our OCT study, embryo hearts were harvested, fixed for a few hours, and optically cleared overnight. On the next day, hearts were imaged (~1 min per heart for 3 datasets taken at different focus depths/orientations i.e. ~20 seconds per dataset acquired) with the OCT system and subsequent identification and segmentation of heart defects took approximately 20 minutes per heart. For 26 embryos, this constitutes less than a day of work in total compared to several days/weeks for histological examination. In addition, by loading the OCT images into AMIRA, 3-D volume renderings of embryo hearts can be created and oriented so that specimens can be compared at a consistent plane or level. Cardiac anomalies can then be easily measured or quantified, which allows for objective comparison of embryos especially in cases where the defects are subtle or too complex for visual identification. Thus in comparison to conventional histological methodologies, by optically slicing the sample rather than physically sectioning it, OCT allows for faster, easier analysis with very little training or expertise required. In addition, OCT technology is now widely available at many major universities and given the very low operational and material costs, there is great potential for its use as an initial screening tool for high-volume embryo models.

There are of course certain limitations to OCT imaging. First, CHD analysis is affected by the degree of optical clearing of the tissue. Currently with tissue clearing, we can visualize approximately 75% of the depth of the ED 8 quail heart which typically has a thickness of a few mm. With the continual optimization of protocols, we expect to overcome such difficulties in future studies and expand our analytical parameters. For example, with more effective optical clearing, we anticipate being able to visualize and segment the entire aortic valve in addition to the pulmonary valve. These techniques are also applicable to other animal models. For example, Xenopus, zebrafish and mouse embryo hearts are more transparent and/or smaller than avian hearts at these late developmental stages which will increase the likelihood that they can be imaged all the way through using OCT imaging and optical clearing protocols. As another limitation, we have observed that blood may accumulate in the ventricular trabeculae or around the atrio-ventricular valve leaflets which can complicate segmentation. This challenging issue can mostly be circumvented by more rapid heart dissections and incubating the sample long enough in the potassium chloride solution to allow more complete expulsion of blood from the cardiac chambers. Finally, although current OCT systems may have limited penetration and resolution compared to

some imaging methods, these parameters will only improve in the future with continued development of the technology. Moreover, the much quicker imaging (~20 seconds per dataset taken), post-processing and analysis protocols associated with OCT recommend the technology as an efficient way to screen embryo models to determine whether it is necessary to use additional imaging methods for further analysis that may require more time, skill, effort and expense.

OCT analysis of our avian model of ethanol exposure revealed a spectrum of cardiac defects, including ventricular septal defects (VSDs) that are common cardiac features associated with FAS with potentially serious consequences. The type and severity of a VSD is important to identify because of the difference in outcome and requisite medical care. Ethanol-exposed embryos presented with both perimembranous VSDs (hole at the top of the septum) and muscular VSDs (described as “Swiss cheese”-like holes in the muscular portion of the septum). Typically, the development of VSDs indicates a failure to fuse of one or more of the following: the endocardial cushions, the conotruncal ridges that eventually form the aortico-pulmonary septum, and the muscular/trabecular portion of the IVS. Muscular VSDs can also occur as a result of excessive re-absorption of tissue during ventricular growth and remodeling. The prognosis can be variable, since a smaller VSD can often spontaneously close during the first few months of postnatal life (Lin et al., 2001). However, larger VSDs can lead to aortic insufficiency and congestive heart failure, especially if accompanied by the presentation of other cardiac anomalies, and often require immediate surgical repair after birth to ensure good long-term outcomes (Glen et al., 2004).

In addition, alterations in vessel size and valve dimensions in a disease or experimental setting can often serve as indicators and/or predictors of abnormal flow or cardiac output. In this model of FAS, total vessel size was reduced significantly for the three branches of the aortic trunk. In previous studies from our group, ethanol exposure led to abnormal cardiac function in the outflow tract (increased retrograde flow) at early embryonic stages (Karunamuni et al., 2014), so presumably there was less forward flow in this region. It may be possible that these early-stage cardiovascular anomalies could be influencing the remodeling of the outflow tract into the major branching arteries. In any case, the decrease in size of the three aortic branches in ethanol-exposed embryos is likely to have a detrimental impact on blood flow to the rest of the body, as well as cerebral blood flow which may contribute to the poor neurodevelopmental outcomes in FAS patients. Furthermore, although there was no significant reduction in diameter for the pulmonary arteries, the presence of a hypoplastic pulmonary valve may precede the development of pulmonary artery-related problems after birth/hatching.

Other hallmarks of this late-stage FAS model included abnormal morphologies and/or reduced volumes of the left AV (mitral) valve. These anomalies can severely impair cardiac function by increasing the leakage of blood back into the left atrium (increased regurgitation), thus reducing cardiac output. Clinically this is analogous to mitral insufficiency, which is the most common form of valvular heart disease (Nkomo et al., 2006) and refers to the incomplete sealing of the valve leaflets during normal valve closure. This phenomenon can lead to serious cardiac events, including dyspnea, decreased exercise capacity, syncope, heart failure, angina and arrhythmias. Surgical repair of the valves is

often the only recourse in most patients (Adams et al., 2006; Enriquez-Sarano et al., 2009) and has yielded good long-term outcomes. However valve repair in young children is more problematic because multiple surgeries may be required during the life of the individual to compensate for growth. It has also been demonstrated that abnormalities in any of the cardiac valves can produce turbulent flow, as a result of altered regurgitation, and promote the growth of micro-lesions on the valve surface (Nishimura, 2002; Faletra, 2013). These often serve as an entry point for microorganisms present in the bloodstream and can lead to bacterial infections e.g. endocarditis (Nishimura, 2002; Faletra, 2013). It would appear therefore that abnormal valvular phenotypes can foreshadow the presentation of cardiac conditions of a graver nature.

It is not yet clear how ethanol is contributing to the development of CHDs in an FAS model. In humans, up to 54% of children diagnosed with FAS can present with CHDs that often require surgical correction and long-term care (E., 1990; Burd et al., 2007), thus necessitating the exploration of the underlying mechanisms. Based on our findings, we can make certain speculations as to the etiology of the ethanol-induced CHDs. The locations of the heart defects observed in our avian system (great vessels, outflow valves, interventricular septum) suggest a partial role for cardiac neural crest cells (CNCCs) that may have been impacted by ethanol exposure, as has been demonstrated for cranial neural crest cells (Cartwright and Smith, 1995b; Cartwright and Smith, 1995a). CNCCs have been shown to migrate into these specific regions of the heart in the avian embryo and their ablation has resulted in similar defects [as reviewed in (Hutson and Kirby, 2003)]. Other candidates for triggering the progression of CHDs include altered molecular signaling and abnormal cardiac function, as well as direct ethanol toxicity (Grummer and Zachman, 1995; Ikonomidou et al., 2000; Ahlgren et al., 2002; Satiroglu-Tufan and Tufan, 2004; Li et al., 2007; Kumar et al., 2009; Serrano et al., 2010; Linask, 2013; Karunamuni et al., 2014). One intriguing area of research that is gaining widespread interest is the effect of ethanol on epigenetics, especially with regards to DNA methylation and gene silencing (Barak et al., 1987; Lieber et al., 1990). Further investigation of these fields is warranted, particularly if we are to develop new therapeutic and/or CHD prevention strategies for FAS.

Conclusions

In summary, we demonstrated the benefits of using OCT to generate valuable data about the FAS model, especially concerning the valvular defects that are often difficult to assess using other technologies. These findings can give clinicians a more complete picture of the CHDs that are associated with an FAS diagnosis, in order to implement a truly effective regimen of treatment. Furthermore, 3-D analysis of CHDs using OCT was conducted in a consistent manner with rapid collection of quantitative and qualitative data. This will be especially useful in studies where the severity of a particular structural abnormality could be correlated with the degree of the experimental manipulation, be it environmental, molecular or functional. With the growing accessibility and relatively low-cost of customizing an OCT system, we anticipate that more developmental biologists will take advantage of this unique opportunity to provide new insight into their own experimental models.

Experimental Procedures

Ethics Statement

IACUC approval was not required for this study which involves the use of avian (quail) embryos that were collected at Embryonic Day 8. Quail embryos typically hatch at Embryonic Day 17. According to IACUC guidelines at Case Western Reserve University, the Policy on the use of Avian Embryos states that "If embryos will be sacrificed prior to 3 days before hatching, the research will not be subject to IACUC review."

Ethanol Exposure

Fertilized quail eggs (*Coturnix coturnix communis*; Boyd's Bird Company, Inc., Pullman, WA) were incubated in a humidified incubator (G.Q.F. Manufacturing Co., Savannah, GA) at 38°C until HH Stage 4-5 (gastrulation), at which stage the embryo has been found to be susceptible to the induction of CHDs (Serrano et al., 2010; Karunamuni et al., 2014). Solutions were injected into the egg using an insulin needle (28 gauge) and holes were sealed with tape before eggs were re-incubated. Experimental eggs were injected with 40 μl of 50% ethanol and control eggs were either injected with 40 μl of saline or left intact. Ethanol dosage was based on previously published protocols (Fang et al., 1987; Bruyere and Kapil, 1990; Bruyere et al., 1994; Serrano et al., 2010) as being equivalent to one binge-like drinking episode in humans (4-5 standard drinks on one occasion) and has reliably produced FAS-associated CHDs (Serrano et al., 2010; Karunamuni et al., 2014).

Optical Clearing

Cohorts of control and ethanol-exposed embryos were allowed to develop until HH stage 34, when the heart has acquired a four-chambered morphology and developed valve leaflets. Hearts from the different exposure groups were dissected, incubated in 0.5M potassium chloride (to relax the heart), washed in phosphate buffered saline, and fixed in formalin. Samples were then optically cleared using the Clear-T protocol, involving a series of increasingly concentrated formamide solutions (20% formamide for 30 minutes, 40% for 30 minutes, 80% for 2 hours, and 95% for 30 minutes and then overnight) (Kuwajima et al., 2013), before being imaged with the OCT system.

OCT Imaging of Hearts

Embryos were imaged using a custom-built Fourier domain OCT system with a quasi-telecentric scanner (Hu and Rollins, 2005; Hu and Rollins, 2007; Ma et al., 2014; Peterson et al., 2014). The OCT light source is a superluminescent diode centered at 1310 nm with a full-width at half-maximum bandwidth of 75 nm. The OCT system uses a linear-in-wavenumber spectrometer and a line-scan camera with a line rate of 47 kHz (Hu and Rollins, 2007). The axial resolution as well as the lateral resolution is approximately 10 μm in tissue (Hu and Rollins, 2005). Thus OCT imaging offers high spatial resolution and extremely high temporal resolution, while providing good penetration depth (1-3 mm in cardiac tissues) (Fujimoto, 2002). For this study, embryo hearts were placed in 95% formamide in a small plastic dish for imaging and an OCT volume (1000 lines/frame, 400 frames/volume) was recorded for each sample. For each heart, 3 volumes were taken: two

from the front focusing on the great vessels and the atrio-ventricular (AV) valves respectively, and one from the back also focusing on the AV valves. On average, it takes approximately 1 minute to acquire the 3 datasets using the OCT system.

Post-processing and Analysis of OCT Images

Customized MATLAB programs (MathWorks; Natick, MA) were used to generate OCT images from the raw data, which were then rendered and analyzed with AMIRA software (FEI Visualization Sciences Group; Burlington, MA). The frontal plane was primarily used for the identification of septal defects while the transverse place was used for the identification of outflow defects and the measurement of vessel diameters and septum thicknesses. Vessel diameters were measured after the immediate branching into the individual arteries. The cardiac valves were also segmented in AMIRA in order to measure their volumes. A few embryos (two controls, one ethanol) could not be analyzed for atrio-ventricular valve defects because excessive blood accumulation around the valve leaflets prevented accurate segmentation.

Acknowledgements

The authors thank Dr. Jennifer Biber for providing clinical perspective. We acknowledge the funding support provided by the National Institute of Health grants R01HL083048, R01HL095717 and R21-HL115373, and the postdoctoral fellowship 14POST19960016 (to GK) provided by the American Heart Association.

Grant support: National Institute of Health grants R01HL083048, R01HL095717 and R21-HL115373, and American Heart Association fellowship 14POST19960016 (to GK)

References

Adams DH, Anyanwu AC, Rahmanian PB, Filsoufi F. Current concepts in mitral valve repair for degenerative disease. Heart Fail Rev. 2006; 11:241–257. [PubMed: 17041764]

Ahlgren SC, Thakur V, Bronner-Fraser M. Sonic hedgehog rescues cranial neural crest from cell death induced by ethanol exposure. Proc Natl Acad Sci U S A. 2002; 99:10476–10481. [PubMed: 12140368]

Asrar Ul Haq M, Layland J, Mutha V, Barlis P. The invasive assessment of coronary atherosclerosis and stents using optical coherence tomography: a clinical update. Heart Asia. 2013; 5:154–161. [PubMed: 24563666]

Barak AJ, Beckenhauer HC, Tuma DJ, Badakhsh S. Effects of prolonged ethanol feeding on methionine metabolism in rat liver. Biochem Cell Biol. 1987; 65:230–233. [PubMed: 3580171]

Berrios-Otero CA, Wadghiri YZ, Nieman BJ, Joyner AL, Turnbull DH. Three-dimensional micro-MRI analysis of cerebral artery development in mouse embryos. Magn Reson Med. 2009; 62:1431–1439. [PubMed: 19859945]

Bruyere HJ Jr. Choudhury S, Nelson E, Stith CE. Cardioteratogenic dose of ethanol in the chick embryo results in albumin ethanol concentrations comparable to human blood alcohol levels. J Appl Toxicol. 1994; 14:33–36. [PubMed: 8157867]

Bruyere HJ Jr. Kapil RP. Cardioteratogenic dose of ethanol in the chick embryo results in egg white concentrations comparable to human blood alcohol levels. J Appl Toxicol. 1990; 10:69–71. [PubMed: 2335714]

Bruyere HJ Jr. Stith CE. Strain-dependent effect of ethanol on ventricular septal defect frequency in White Leghorn chick embryos. Teratology. 1993; 48:299–303. [PubMed: 8278929]

Burd L, Deal E, Rios R, Adickes E, Wynne J, Klug MG. Congenital heart defects and fetal alcohol spectrum disorders. Congenit Heart Dis. 2007; 2:250–255. [PubMed: 18377476]

Cartwright MM, Smith SM. Increased cell death and reduced neural crest cell numbers in ethanol-exposed embryos: partial basis for the fetal alcohol syndrome phenotype. Alcohol Clin Exp Res. 1995a; 19:378–386. [PubMed: 7625573]

Cartwright MM, Smith SM. Stage-dependent effects of ethanol on cranial neural crest cell development: partial basis for the phenotypic variations observed in fetal alcohol syndrome. Alcohol Clin Exp Res. 1995b; 19:1454–1462. [PubMed: 8749810]

Cheng KC, Xin X, Clark DP, La Riviere P. Whole-animal imaging, gene function, and the Zebrafish Phenome Project. Curr Opin Genet Dev. 2011; 21:620–629. [PubMed: 21963132]

Cleary JO, Price AN, Thomas DL, Scambler PJ, Kyriakopoulou V, McCue K, Schneider JE, Ordidge RJ, Lythgoe MF. Cardiac phenotyping in ex vivo murine embryos using microMRI. NMR Biomed. 2009; 22:857–866. [PubMed: 19598179]

Daft PA, Johnston MC, Sulik KK. Abnormal heart and great vessel development following acute ethanol exposure in mice. Teratology. 1986; 33:93–104. [PubMed: 3738814]

Davis AM, Rothenberg FG, Shepherd N, Izatt JA. In vivo spectral domain optical coherence tomography volumetric imaging and spectral Doppler velocimetry of early stage embryonic chicken heart development. J Opt Soc Am A Opt Image Sci Vis. 2008; 25:3134–3143. [PubMed: 19037405]

deAlmeida A, McQuinn T, Sedmera D. Increased ventricular preload is compensated by myocyte proliferation in normal and hypoplastic fetal chick left ventricle. Circ Res. 2007; 100:1363–1370. [PubMed: 17413043]

Degenhardt K, Wright AC, Horng D, Padmanabhan A, Epstein JA. Rapid 3D phenotyping of cardiovascular development in mouse embryos by micro-CT with iodine staining. Circ Cardiovasc Imaging. 2010; 3:314–322. [PubMed: 20190279]

Drexler, W.; Fujimoto, JG. Optical coherence tomography: technology and applications. Vol. xxix. Springer; Berlin; New York: 2008a. p. 1346

Drexler W, Fujimoto JG. State-of-the-art retinal optical coherence tomography. Prog Retin Eye Res. 2008b; 27:45–88. [PubMed: 18036865]

E, A. Fetal Alcohol syndrome. Oradell, NJ: 1990.

Enriquez-Sarano M, Akins CW, Vahanian A. Mitral regurgitation. Lancet. 2009; 373:1382–1394. [PubMed: 19356795]

Faletra, FF. Echocardiography in Mitral Valve Disease. Springer; 2013.

Fang TT, Bruyere HJ Jr. Kargas SA, Nishikawa T, Takagi Y, Gilbert EF. Ethyl alcohol-induced cardiovascular malformations in the chick embryo. Teratology. 1987; 35:95–103. [PubMed: 3563941]

Fernandez EJ, Hermann B, Povazay B, Unterhuber A, Sattmann H, Hofer B, Ahnelt PK, Drexler W. Ultrahigh resolution optical coherence tomography and pancorrection for cellular imaging of the living human retina. Opt Express. 2008; 16:11083–11094. [PubMed: 18648422]

Ferrante G, Presbitero P, Whitbourn R, Barlis P. Current applications of optical coherence tomography for coronary intervention. Int J Cardiol. 2013; 165:7–16. [PubMed: 22405134]

French J, Gingles N, Stewart J, Woodhouse N. Use of magnetic resonance imaging (MRI) and micro-computed tomography (micro-CT) in the morphological examination of rat and rabbit fetuses from embryo-fetal development studies. Reprod Toxicol. 2010; 30:292–300. [PubMed: 20452417]

Fujimoto, JG. Optical conherence tomography: Introduction. In: Bouma, BE.; Tearney, GJ., editors. Handbook of Optical Coherence Tomography. Marcel Dekker, Inc.; New York: 2002. p. 1-40.

Garita B, Jenkins MW, Han M, Zhou C, Vanauker M, Rollins AM, Watanabe M, Fujimoto JG, Linask KK. Blood flow dynamics of one cardiac cycle and relationship to mechanotransduction and trabeculation during heart looping. Am J Physiol Heart Circ Physiol. 2011; 300:H879–891. [PubMed: 21239637]

Geyer SH, Mohun TJ, Weninger WJ. Visualizing vertebrate embryos with episcopic 3D imaging techniques. ScientificWorldJournal. 2009; 9:1423–1437. [PubMed: 20024516]

Glen S, Burns J, Bloomfield P. Prevalence and development of additional cardiac abnormalities in 1448 patients with congenital ventricular septal defects. Heart. 2004; 90:1321–1325. [PubMed: 15486133]

Grummer MA, Zachman RD. Prenatal ethanol consumption alters the expression of cellular retinol binding protein and retinoic acid receptor mRNA in fetal rat embryo and brain. Alcohol Clin Exp Res. 1995; 19:1376–1381. [PubMed: 8749798]

Gu S, Jenkins MW, Watanabe M, Rollins AM. High-speed optical coherence tomography imaging of the beating avian embryonic heart. Cold Spring Harb Protoc. 20112011 pdb top98.

Hamburger V, Hamilton HL. A series of normal stages in the development of the chick embryo. J Morphol. 1951; 88:49–92. [PubMed: 24539719]

Happel CM, Thrane L, Thommes J, Manner J, Yelbuz TM. Integration of an optical coherence tomography (OCT) system into an examination incubator to facilitate in vivo imaging of cardiovascular development in higher vertebrate embryos under stable physiological conditions. Ann Anat. 2011; 193:425–435. [PubMed: 21641190]

Hiraiwa N, Ishimoto M, Yasue H. Examination of the mouse embryo by micro-CT. Exp Anim. 2013; 62:57–61. [PubMed: 23357947]

Hogers B, van der Weerd L, Olofsen H, van der Graaf LM, DeRuiter MC, Gittenberger-de Groot AC, Poelmann RE. Non-invasive tracking of avian development in vivo by MRI. NMR Biomed. 2009; 22:365–373. [PubMed: 19003815]

Hu Z, Rollins A. Quasi-telecentric optical design of a microscope-compatible OCT scanner. Opt Express. 2005; 13:6407–6415. [PubMed: 19498654]

Hu Z, Rollins AM. Fourier domain optical coherence tomography with a linear-in-wavenumber spectrometer. Opt Lett. 2007; 32:3525–3527. [PubMed: 18087530]

Hutson MR, Kirby ML. Neural crest and cardiovascular development: a 20-year perspective. Birth Defects Res C Embryo Today. 2003; 69:2–13. [PubMed: 12768653]

Ide T, Wang J, Tao A, Leng T, Kymionis GD, O'Brien TP, Yoo SH. Intraoperative use of three-dimensional spectral-domain optical coherence tomography. Ophthalmic Surg Lasers Imaging. 2010; 41:250–254. [PubMed: 20307045]

Ikonomidou C, Bittigau P, Ishimaru MJ, Wozniak DF, Koch C, Genz K, Price MT, Stefovska V, Horster F, Tenkova T, Dikranian K, Olney JW. Ethanol-induced apoptotic neurodegeneration and fetal alcohol syndrome. Science. 2000; 287:1056–1060. [PubMed: 10669420]

Jenkins MW, Adler DC, Gargesha M, Huber R, Rothenberg F, Belding J, Watanabe M, Wilson DL, Fujimoto JG, Rollins AM. Ultrahigh-speed optical coherence tomography imaging and visualization of the embryonic avian heart using a buffered Fourier Domain Mode Locked laser. Opt Express. 2007a; 15:6251–6267. [PubMed: 19546930]

Jenkins MW, Chughtai OQ, Basavanhally AN, Watanabe M, Rollins AM. In vivo gated 4D imaging of the embryonic heart using optical coherence tomography. J Biomed Opt. 2007b; 12:030505. [PubMed: 17614708]

Jenkins MW, Watanabe M, Rollins AM. Longitudinal Imaging of Heart Development with Optical Coherence Tomography. IEEE Photonics Society (IPS) Journal of Selected Topics in Quantum Electronics. 2012

Karunamuni G, Gu S, Doughman YQ, Peterson LM, Mai K, McHale Q, Jenkins MW, Linask KK, Rollins AM, Watanabe M. Ethanol exposure alters early cardiac function in the looping heart: a mechanism for congenital heart defects? Am J Physiol Heart Circ Physiol. 2014; 306:H414–421. [PubMed: 24271490]

Konig K. Multiphoton microscopy in life sciences. J Microsc. 2000; 200:83–104. [PubMed: 11106949]

Kumar S, Porcu P, Werner DF, Matthews DB, Diaz-Granados JL, Helfand RS, Morrow AL. The role of GABA(A) receptors in the acute and chronic effects of ethanol: a decade of progress. Psychopharmacology (Berl). 2009; 205:529–564. [PubMed: 19455309]

Kuwajima T, Sitko AA, Bhansali P, Jurgens C, Guido W, Mason C. ClearT: a detergent- and solvent-free clearing method for neuronal and non-neuronal tissue. Development. 2013; 140:1364–1368. [PubMed: 23444362]

Larina IV, Sudheendran N, Ghosn M, Jiang J, Cable A, Larin KV, Dickinson ME. Live imaging of blood flow in mammalian embryos using Doppler swept-source optical coherence tomography. J Biomed Opt. 2008; 13:060506. [PubMed: 19123647]

Li YX, Yang HT, Zdanowicz M, Sicklick JK, Qi Y, Camp TJ, Diehl AM. Fetal alcohol exposure impairs Hedgehog cholesterol modification and signaling. Lab Invest. 2007; 87:231–240. [PubMed: 17237799]

Lieber CS, Casini A, DeCarli LM, Kim CI, Lowe N, Sasaki R, Leo MA. S-adenosyl-L-methionine attenuates alcohol-induced liver injury in the baboon. Hepatology. 1990; 11:165–172. [PubMed: 2307395]

Lin MH, Wang NK, Hung KL, Shen CT. Spontaneous closure of ventricular septal defects in the first year of life. J Formos Med Assoc. 2001; 100:539–542. [PubMed: 11678004]

Linask KK. The heart-placenta axis in the first month of pregnancy: induction and prevention of cardiovascular birth defects. J Pregnancy. 20132013:320413. [PubMed: 23691322]

Liu A, Yin X, Shi L, Li P, Thornburg KL, Wang R, Rugonyi S. Biomechanics of the chick embryonic heart outflow tract at HH18 using 4D optical coherence tomography imaging and computational modeling. PLoS One. 2012; 7:e40869. [PubMed: 22844414]

Liu X, Tobita K, Francis RJ, Lo CW. Imaging techniques for visualizing and phenotyping congenital heart defects in murine models. Birth Defects Res C Embryo Today. 2013; 99:93–105. [PubMed: 23897594]

Lu Y, James TN, Bootsma M, Terasaki F. Histological organization of the right and left atrioventricular valves of the chicken heart and their relationship to the atrioventricular Purkinje ring and the middle bundle branch. Anat Rec. 1993; 235:74–86. [PubMed: 8417630]

Ma P, Wang YT, Gu S, Watanabe M, Jenkins MW, Rollins AM. Three-dimensional correction of conduction velocity in the embryonic heart using integrated optical mapping and optical coherence tomography. J Biomed Opt. 2014; 19:76004. [PubMed: 24996663]

McQuinn TC, Bratoeva M, Dealmeida A, Remond M, Thompson RP, Sedmera D. High-frequency ultrasonographic imaging of avian cardiovascular development. Dev Dyn. 2007; 236:3503–3513. [PubMed: 17948299]

Memon S, Pratten MK. Developmental toxicity of ethanol in chick heart in ovo and in micromass culture can be prevented by addition of vitamin C and folic acid. Reprod Toxicol. 2009; 28:262–269. [PubMed: 19473809]

Mohun TJ, Weninger WJ. Episcopic three-dimensional imaging of embryos. Cold Spring Harb Protoc. 2012; 2012:641–646. [PubMed: 22661435]

Moran CM, Thomson AJ, Rog-Zielinska E, Gray GA. High-resolution echocardiography in the assessment of cardiac physiology and disease in preclinical models. Exp Physiol. 2013; 98:629–644. [PubMed: 23118017]

Nieman BJ, Turnbull DH. Ultrasound and magnetic resonance microimaging of mouse development. Methods Enzymol. 2010; 476:379–400. [PubMed: 20691877]

Nishimura RA. Cardiology patient pages. Aortic valve disease. Circulation. 2002; 106:770–772. [PubMed: 12176943]

Nkomo VT, Gardin JM, Skelton TN, Gottdiener JS, Scott CG, Enriquez-Sarano M. Burden of valvular heart diseases: a population-based study. Lancet. 2006; 368:1005–1011. [PubMed: 16980116]

Pawley, JB. Handbook of biological confocal microscopy. Springer; New York: 2006. 1 online resource (985 blz.)

Peterson LM, Gu S, Jenkins MW, Rollins AM. Orientation-independent rapid pulsatile flow measurement using dual-angle Doppler OCT. Biomed Opt Express. 2014; 5:499–514. [PubMed: 24575344]

Petiet AE, Kaufman MH, Goddeeris MM, Brandenburg J, Elmore SA, Johnson GA. High-resolution magnetic resonance histology of the embryonic and neonatal mouse: a 4D atlas and morphologic database. Proc Natl Acad Sci U S A. 2008; 105:12331–12336. [PubMed: 18713865]

Prati F, Jenkins MW, Di Giorgio A, Rollins AM. Intracoronary optical coherence tomography, basic theory and image acquisition techniques. Int J Cardiovasc Imaging. 2011; 27:251–258. [PubMed: 21327912]

Ritman EL. Current status of developments and applications of micro-CT. Annu Rev Biomed Eng. 2011; 13:531–552. [PubMed: 21756145]

Rosenthal J, Mangal V, Walker D, Bennett M, Mohun TJ, Lo CW. Rapid high resolution three dimensional reconstruction of embryos with episcopic fluorescence image capture. Birth Defects Res C Embryo Today. 2004; 72:213–223. [PubMed: 15495188]

Rugonyi S, Shaut C, Liu A, Thornburg K, Wang RK. Changes in wall motion and blood flow in the outflow tract of chick embryonic hearts observed with optical coherence tomography after outflow tract banding and vitelline-vein ligation. Phys Med Biol. 2008; 53:5077–5091. [PubMed: 18723935]

Santi PA. Light sheet fluorescence microscopy: a review. J Histochem Cytochem. 2011; 59:129–138. [PubMed: 21339178]

Satiroglu-Tufan NL, Tufan AC. Amelioration of ethanol-induced growth retardation by all-trans-retinoic acid and alpha-tocopherol in shell-less culture of the chick embryo. Reprod Toxicol. 2004; 18:407–412. [PubMed: 15082076]

Schambach SJ, Bag S, Schilling L, Groden C, Brockmann MA. Application of micro-CT in small animal imaging. Methods. 2010; 50:2–13. [PubMed: 19706326]

Serrano M, Han M, Brinez P, Linask KK. Fetal alcohol syndrome: cardiac birth defects in mice and prevention with folate. Am J Obstet Gynecol. 2010; 203:75 e77–75 e15. [PubMed: 20451895]

Sharpe J, Ahlgren U, Perry P, Hill B, Ross A, Hecksher-Sorensen J, Baldock R, Davidson D. Optical projection tomography as a tool for 3D microscopy and gene expression studies. Science. 2002; 296:541–545. [PubMed: 11964482]

Shen Y, Leatherbury L, Rosenthal J, Yu Q, Pappas MA, Wessels A, Lucas J, Siegfried B, Chatterjee B, Svenson K, Lo CW. Cardiovascular phenotyping of fetal mice by noninvasive high-frequency ultrasound facilitates recovery of ENU-induced mutations causing congenital cardiac and extracardiac defects. Physiol Genomics. 2005; 24:23–36. [PubMed: 16174781]

Simpson JM, Miller O. Three-dimensional echocardiography in congenital heart disease. Arch Cardiovasc Dis. 2011; 104:45–56. [PubMed: 21276577]

Sohrab M, Fawzi A. Review of En-Face Choroidal Imaging Using Spectral-Domain Optical Coherence Tomography. Med Hypothesis Discov Innov Ophthalmol. 2013; 2:69–73. [PubMed: 24600646]

Spurney CF, Lo CW, Leatherbury L. Fetal mouse imaging using echocardiography: a review of current technology. Echocardiography. 2006; 23:891–899. [PubMed: 17069613]

Sulik KK, Johnston MC, Daft PA, Russell WE, Dehart DB. Fetal alcohol syndrome and DiGeorge anomaly: critical ethanol exposure periods for craniofacial malformations as illustrated in an animal model. Am J Med Genet Suppl. 1986; 2:97–112. [PubMed: 3146306]

Swoger J, Pampaloni F, Stelzer EH. Light-sheet-based fluorescence microscopy for three-dimensional imaging of biological samples. Cold Spring Harb Protoc. 20142014:1–8. [PubMed: 24371323]

Tao YK, Ehlers JP, Toth CA, Izatt JA. Intraoperative spectral domain optical coherence tomography for vitreoretinal surgery. Opt Lett. 2010; 35:3315–3317. [PubMed: 20967051]

Tearney GJ, Regar E, Akasaka T, Adriaenssens T, Barlis P, Bezerra HG, Bouma B, Bruining N, Cho JM, Chowdhary S, Costa MA, de Silva R, Dijkstra J, Di Mario C, Dudek D, Falk E, Feldman MD, Fitzgerald P, Garcia-Garcia HM, Gonzalo N, Granada JF, Guagliumi G, Holm NR, Honda Y, Ikeno F, Kawasaki M, Kochman J, Koltowski L, Kubo T, Kume T, Kyono H, Lam CC, Lamouche G, Lee DP, Leon MB, Maehara A, Manfrini O, Mintz GS, Mizuno K, Morel MA, Nadkarni S, Okura H, Otake H, Pietrasik A, Prati F, Raber L, Radu MD, Rieber J, Riga M, Rollins A, Rosenberg M, Sirbu V, Serruys PW, Shimada K, Shinke T, Shite J, Siegel E, Sonoda S, Suter M, Takarada S, Tanaka A, Terashima M, Thim T, Uemura S, Ughi GJ, van Beusekom HM, van der Steen AF, van Es GA, van Soest G, Virmani R, Waxman S, Weissman NJ, Weisz G. Consensus standards for acquisition, measurement, and reporting of intravascular optical coherence tomography studies: a report from the International Working Group for Intravascular Optical Coherence Tomography Standardization and Validation. J Am Coll Cardiol. 2012; 59:1058–1072. [PubMed: 22421299]

Tobita K, Liu X, Lo CW. Imaging modalities to assess structural birth defects in mutant mouse models. Birth Defects Res C Embryo Today. 2010; 90:176–184. [PubMed: 20860057]

Vignali L, Solinas E, Emanuele E. Research and clinical applications of optical coherence tomography in invasive cardiology: a review. Curr Cardiol Rev. 2014; 10:369–376. [PubMed: 24893934]

Weninger WJ, Mohun T. Phenotyping transgenic embryos: a rapid 3-D screening method based on episcopic fluorescence image capturing. Nat Genet. 2002; 30:59–65. [PubMed: 11743576]

Weninger WJ, Mohun TJ. Three-dimensional analysis of molecular signals with episcopic imaging techniques. Methods Mol Biol. 2007; 411:35–46. [PubMed: 18287637]

Yelbuz TM, Choma MA, Thrane L, Kirby ML, Izatt JA. Optical coherence tomography: a new high-resolution imaging technology to study cardiac development in chick embryos. Circulation. 2002a; 106:2771–2774. [PubMed: 12451001]

Yelbuz TM, Leatherbury L, Wolfe RR, Loewy R, Kirby ML. Images in cardiovascular medicine. Time-lapse study with high speed video camera in the early embryonic chick heart to visualize a time window of normal and abnormal heart development. Circulation. 2002b; 106:e44–45. [PubMed: 12208810]

Yelbuz TM, Wessel A, Kirby ML. Studies on morphogenesis and visualization of the early embryonic heart with regard to the development of conotruncal heart defects. Z Kardiol. 2004; 93:583–594. [PubMed: 15338144]

Yu Q, Shen Y, Chatterjee B, Siegfried BH, Leatherbury L, Rosenthal J, Lucas JF, Wessels A, Spurney CF, Wu YJ, Kirby ML, Svenson K, Lo CW. ENU induced mutations causing congenital cardiovascular anomalies. Development. 2004; 131:6211–6223. [PubMed: 15548583]

Zouagui T, Chereul E, Janier M, Odet C. 3D MRI heart segmentation of mouse embryos. Comput Biol Med. 2010; 40:64–74. [PubMed: 19939358]

Key findings

- We used optical coherence tomography (OCT), a novel biophotonic tool, to analyze congenital heart defects (CHDs) in an embryonic disease model.
- Avian embryos developed CHDs associated with Fetal Alcohol Syndrome after being exposed to binge volumes of ethanol at gastrulation.
- OCT allowed for the rapid, consistent identification of CHDs such as ventricular septal defects and outflow defects.
- Using OCT images, we measured valve volume, interventricular septum thickness and vessel diameters which were significantly reduced after ethanol exposure.
- This user-friendly, cost-effective technique will be invaluable to developmental biologists seeking to streamline the analysis of embryonic models with the added benefit of precise, reliable quantification.

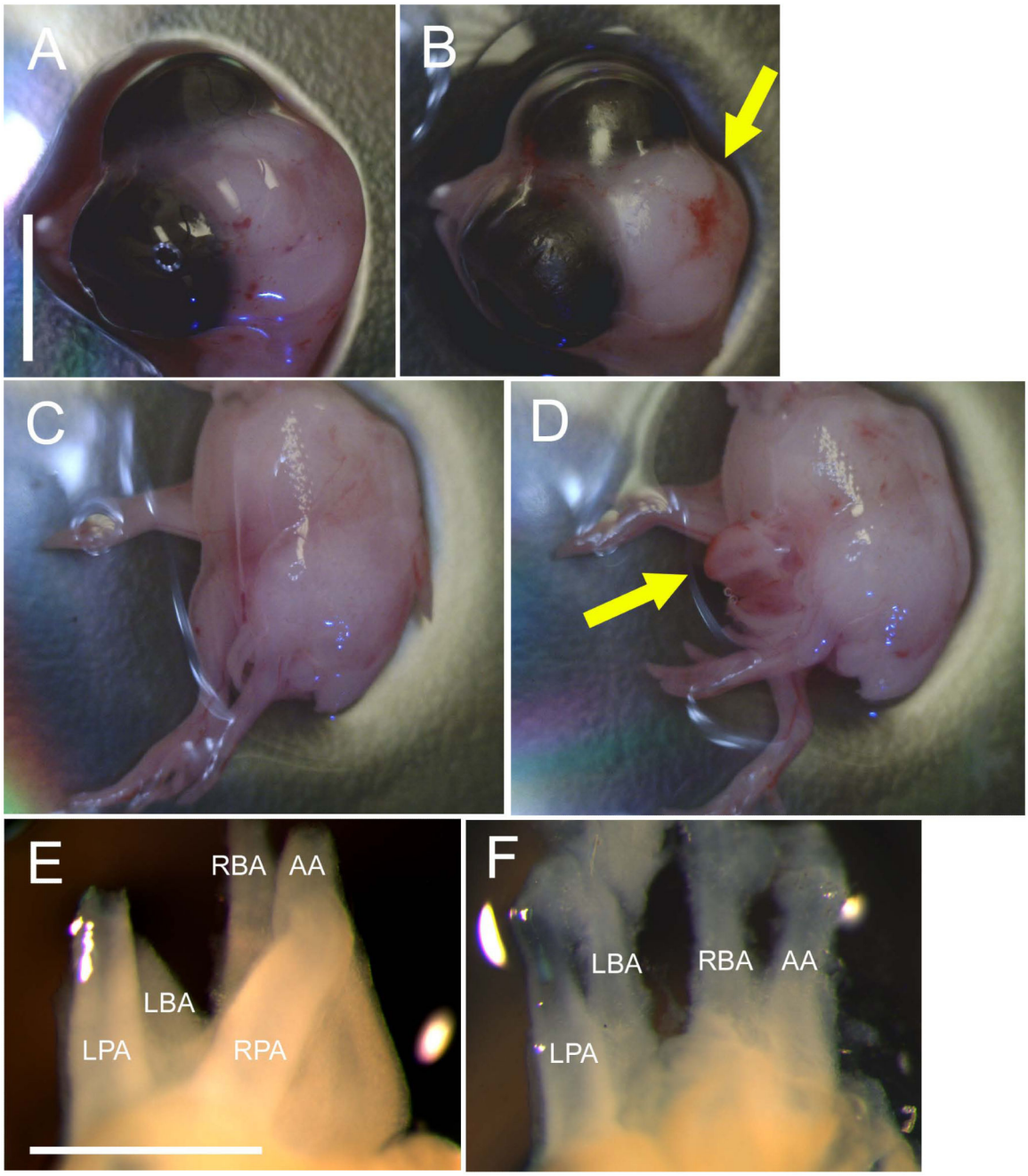

Figure 1. Head, body and cardiac defects after ethanol exposure in the quail embryo

(A) Control embryo with no head defects and (B) ethanol-exposed embryo with cranial folds that failed to fuse, leaving brain tissue exposed (yellow arrow). Scale bar in A applies for A-D and = 0.5 cm. (C) Control embryo with fully fused chest wall and (D) ethanol-exposed embryo with chest wall that failed to fuse, exposing internal organs such as the heart (yellow arrow). (E) Control heart with all five major arterial branches (as viewed from the back) and (F) ethanol-exposed heart with only four major arteries, in this case missing the RPA. Scale

bar = 1 mm. LBA = left brachiocephalic artery, RBA = right brachiocephalic artery, AA = aortic arch, LPA = left pulmonary artery, RPA = right pulmonary artery.

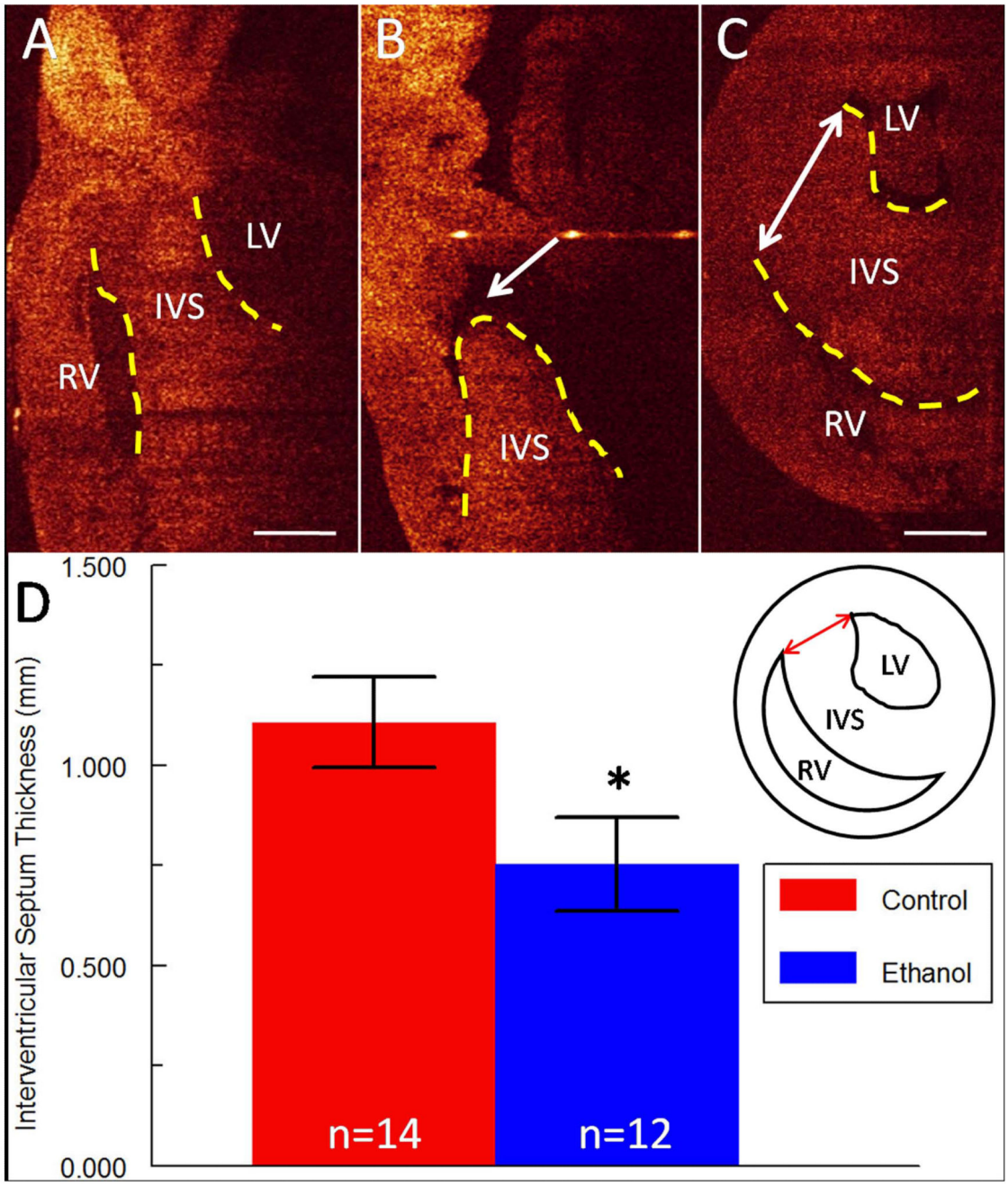

Figure 2. Defects of the interventricular septum (IVS; delineated with yellow dotted lines) after ethanol exposure

(A) IVS in a sagittal OCT slice of a control embryo. LV = left ventricle, RV = right ventricle. Scale bar = 0.5 mm. (B) Perimembranous VSD (arrow) in heart of ethanol-exposed embryo. (C) Double-sided arrow indicates how IVS thickness was measured in a transverse OCT slice of the heart in a control embryo. Scale bar = 0.5 mm. (D) Bar graph of IVS thickness which was significantly reduced (* $p < 0.05$) in ethanol-exposed embryos. Inset shows graphical depiction of IVS measurement (red double-sided arrow).

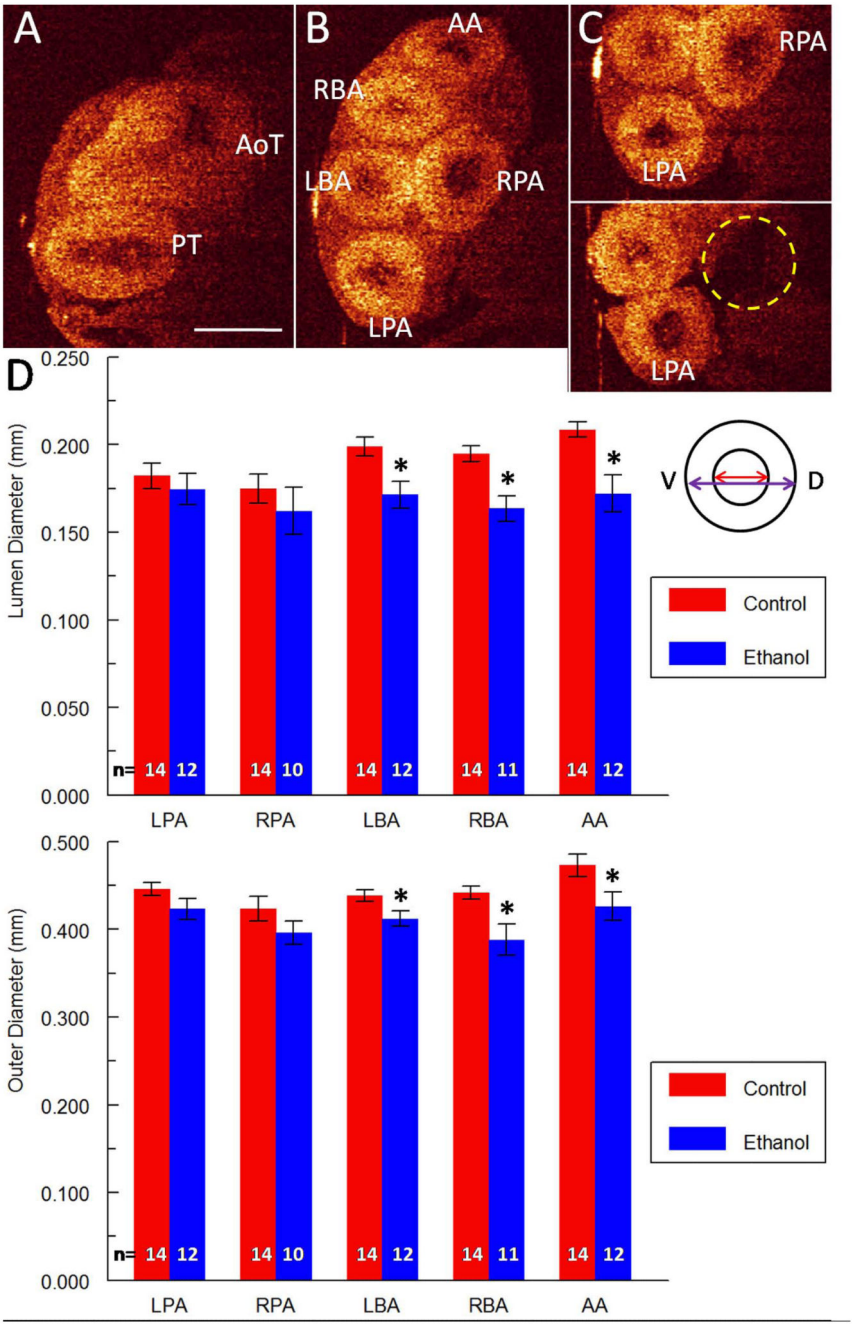

Figure 3. Defects of the outflow tract after ethanol exposure

(A) Aortic trunk (AoT) and pulmonary trunk (PT) from a transverse section of a control heart. Scale bar = 0.5 mm. (B) In the same control heart, aortic trunk branches into left brachiocephalic artery (LBA), right brachiocephalic artery (RBA) and aortic arch (AA). Pulmonary trunk branches into left pulmonary artery (LPA) and right pulmonary artery (RPA). (C) Top panel shows both pulmonary arteries of a control heart. Bottom panel shows a missing RPA (dotted yellow circle) for an ethanol-exposed embryo. (D) Bar graphs of lumenal and outer diameters for the five branching arteries in control and ethanol-exposed

embryos. Significantly reduced diameters were observed for three of the five vessels: the LBA, RBA and AA. Inset depicts example measurements of the lumenal diameter (red double-sided arrow) and outer diameter (purple double-sided arrow) for a vessel. V and D in inset indicate the ventral-dorsal direction. * indicates p-value < 0.05.

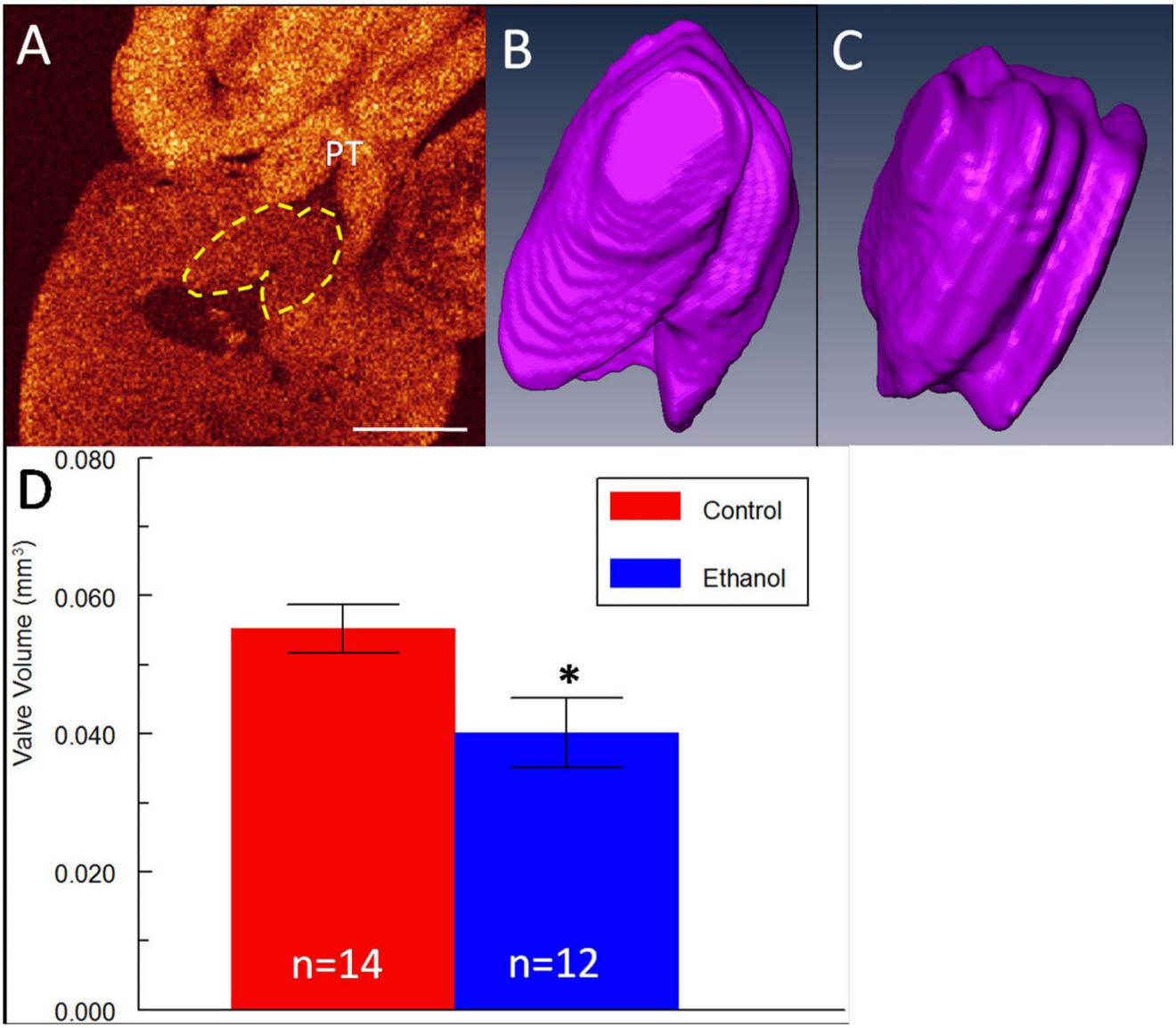

Figure 4. Defects of the developing pulmonary (semilunar) valve in ethanol-exposed embryos

(A) Pulmonary valve (yellow dotted line) in frontal OCT slice of a control heart. PT = pulmonary trunk. Scale bar = 0.5 mm. (B) AMIRA 3-D reconstruction of the pulmonary valve of a control embryo. (C) AMIRA 3-D reconstruction of the pulmonary valve of an ethanol-exposed embryo. (D) Bar graph of pulmonary valve volumes in control and ethanol-exposed embryos. Reduced valvular volumes were observed after ethanol exposure. * indicates p-value < 0.05.

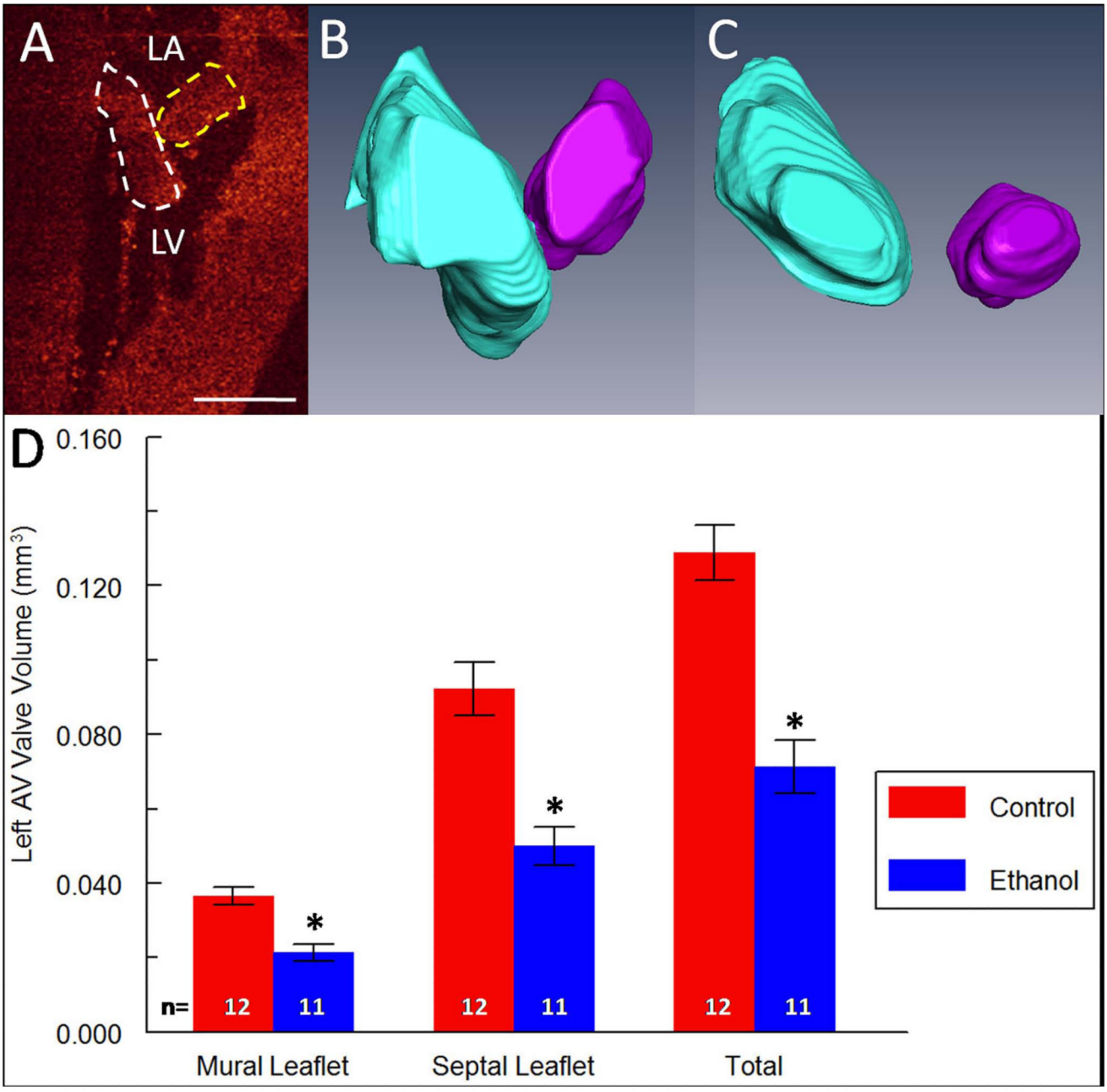

Figure 5. Defects of the left atrio-ventricular (AV) valve in ethanol-exposed embryos

(A) Septal leaflet (white dotted lines) and mural leaflet (yellow dotted lines) of the left AV valve in a frontal OCT slice of a control heart. Speckles around leaflets are blood cells in the ventricular chamber. LA = left atrium, LV = left ventricle. Scale bar = 0.5 mm. (B) 3-D reconstruction of the septal leaflet (blue) and the mural leaflet (purple) of left AV valve in a control embryo. (C) 3-D reconstruction of the septal leaflet (blue) and the mural leaflet (purple) of left AV valve in an ethanol-exposed embryo. For this embryo, the leaflets of the left AV valve did not meet. (D) Bar graph of mural leaflet volume, septal leaflet volume,

and total volume in control and ethanol-exposed embryos. Reduced valvular volumes were observed after ethanol exposure. * indicates p-value < 0.05.

Table 1

Summary of embryo phenotypes at ED 8 (HH Stage 34)

VSD = ventricular septal defect, DORV = double outlet right ventricle.

	Controls	Ethanols
Survival rate	82%	52%
Number of survivors	14	12
Normal head/body	14 (100%)	7 (58%)
Head defects	0 (0%)	2 (17%)
Body defects	0 (0%)	4 (33%)
Normal heart	14 (100%)	5 (42%)
VSDs	0 (0%)	5 (42%)
Missing great vessel	0 (0%)	3 (25%)
DORV	0 (0%)	1 (8%)
Misaligned aorta	0 (0%)	1 (8%)
Hypoplastic right ventricle	0 (0%)	1 (8%)
Abnormal rotation of ventricle	0 (0%)	1 (8%)

Table 2
Defects of ethanol-exposed embryos at ED 8 (HH stage 34)

Note that Embryos #6 and #9 had no obvious head or body defects but developed great vessel abnormalities. VSD = ventricular septal defect, DORV = double outlet right ventricle, RPA = right pulmonary artery, RBA = right brachiocephalic artery.

Embryo #	Head defect	Body defect	Types of cardiac defects
Embryo #1	Yes	No	Muscular VSD
Embryo #2	Yes	Yes	Perimembranous VSD
Embryo #3	No	Yes	Missing RPA, DORV, muscular VSD
Embryo #4	No	No	
Embryo #5	No	No	
Embryo #6	No	No	Missing RPA
Embryo #7	No	No	
Embryo #8	No	No	
Embryo #9	No	No	Missing RBA, misaligned aorta, perimembranous VSD, abnormal rotation of ventricle
Embryo #10	No	No	
Embryo #11	No	Yes	Hypoplastic right ventricle
Embryo #12	No	Yes	Muscular VSD